Forest Service
U.S. DEPARTMENT OF AGRICULTURE

Forest Products Laboratory | Research Note FPL-RN-434 | August 2026

Investigation of the Material Properties of Acid-Activated Biochar Produced Via Low-Temperature Pyrolysis

Radhika Panickar
Roderquita K. Moore
Derrick Dean

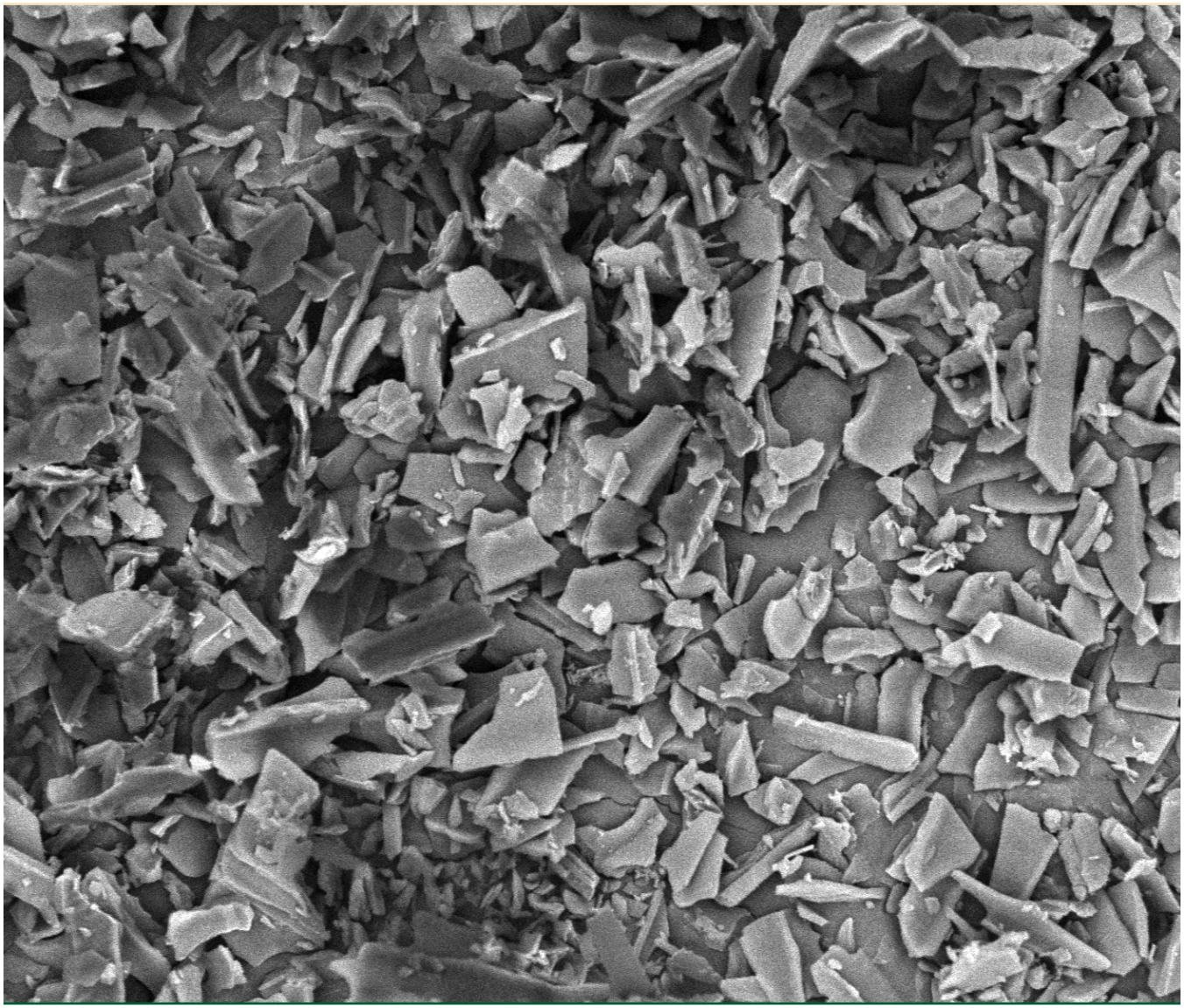

Citation

Panickar, Radhika; Moore, Roderquita K.; Dean, Derrick. 2026. Investigation of the material properties of acid-activated biochar produced via low-temperature pyrolysis. Res. Note FPL-RN-434. Madison, WI: U.S. Department of Agriculture, Forest Service, Forest Products Laboratory. 10 p. https://doi.org/10.2737/FPL-RN-434.

Abstract

This study aims to improve the physical properties of biochar (BC) produced through pyrolysis at 300 °C by employing acid activation. Four acids—nitric acid (HNO_3), hydrochloric acid (HCl), phosphoric acid (H_3PO_4), and sulfuric acid (H_2SO_4)—were used to activate the BC. The acid-activated BC was then characterized to assess the effects of the treatments. Brunauer–Emmett–Teller (BET) analysis indicated a 34 percent increase in surface area for BC activated with H_3PO_4. Fourier transform infrared (FTIR) spectroscopy analysis revealed shifts in peak positions and changes in the functional groups present on the BC for different acids post-treatment. Raman spectroscopy showed a low defect ratio of 0.82, and thermogravimetric analysis (TGA) demonstrated enhanced thermal stability for the H_3PO_4-activated sample. Of the acids tested, H_3PO_4 activation resulted in the most significant improvement in the properties of the biochar.

Keywords: biochar, pyrolysis, acid activation, thermomechanical properties, polymer extrusion

Contents

Abbreviations

ABC	Acid-activated biochar
BC	Biochar
BC_BM	Ball-milled biochar
BET	Brunauer–Emmett–Teller analysis
FTIR	Fourier transform infrared spectroscopy
SEM	Scanning electron microscopy
TGA	Thermogravimetric analysis
XRD	X-ray diffraction

Authors

Radhika Panickar, Alabama State University, Montgomery, Alabama

Roderquita Moore, U.S. Department of Agriculture, Forest Service, Forest Products Laboratory, Madison, Wisconsin, roderquita.k.moore@usda.gov

Derrick Dean, Alabama State University, Montgomery, Alabama

Cover: Scanning electronic microscopy (SEM) image of biochar activated with H_3PO_4. Image by Radhika Panickar/Alabama State University.

Published by

USDA Forest Service, Forest Products Laboratory
One Gifford Pinchot Drive
Madison, WI 53275
(608) 231-9200
August 2026

Visit the Forest Products Laboratory website at https://research.fs.usda.gov/fpl.

The Forest Products Laboratory is maintained in cooperation with the University of Wisconsin.

Introduction

Biochar (BC) is a form of black carbon typically produced through the pyrolysis or carbonization of various biomass materials, such as agricultural waste, wood residues, and plant matter (Uroić Štefanko and Leszczynska 2020, Yaashikaa et al. 2020). The synthesis of BC plays a crucial role in waste management by transforming agricultural and forestry residues into high-value materials. The efficiency and application of BC can vary significantly depending on the type of biomass used and the specific temperature and pressure conditions during pyrolysis. The specific operating parameters during pyrolysis have a significant importance in the quality and quantity of BC synthesis (Leng and Huang 2018).

Operating temperature during the pyrolysis process profoundly influences the properties of the biochar synthesized. It has been reported that a slow heating rate and pyrolysis temperatures below 450 °C result in a high BC yield, whereas slightly higher temperatures combined with an intermediate heating rate tend to produce a high yield of bio-oil. In contrast, temperatures above 800 °C lead to low yields with carbon-rich products (Roshan et al. 2023, Tan and Yuan 2019). Owing to the high BC yield from low-temperature slow pyrolysis, the resulting BC retains a high organic carbon content, indicating minimal carbon loss during the pyrolysis process. This high carbon content contributes to improved physical, chemical, and biological properties that notably enhance water retention, cation exchange capacity, and microbial activity, respectively (Bo et al. 2023, da Silva et al. 2025).

Biochar produced through low-temperature pyrolysis has extensive applications in agriculture (Gaskin et al. 2008, Pariyar et al. 2020). This type of BC retains nutrients and organic compounds that enhance soil fertility, water retention, and microbial activity. These benefits contribute to improved growing conditions, ultimately boosting grain yield. Gaskin et al. (2008) reported that incorporating BC into fertilizers significantly enhanced nitrogen and phosphorus retention in soil. However, BC produced at low-temperature pyrolysis has limited use in other applications due to residual contaminations, its lower carbon content and relatively poor surface area and porosity, and the presence of volatile compounds.

The surface area and porosity of biochar play a crucial role in determining its suitability for engineering and industrial applications (Tan and Yuan 2019). Enhancing these properties can significantly broaden the potential uses of biochar in various fields (Leng et al. 2021, Skic et al. 2024). Studies have reported acid activation of BC produced via high-temperature pyrolysis to enhance surface area and porosity (Esteves et al. 2013, Handiso et al. 2024, Nzediegwu et al. 2022). However, detailed material characterization of acid-activated BC (using HNO_3, HCl, H_3PO_4, or H_2SO_4) synthesized through low-temperature pyrolysis remains unreported. Considering the critical role of surface area and porosity in biochar applications, the present study involves the chemical activation of low temperature pyrolysis BC to enhance these properties. To achieve this, BC was treated with various acids, and the effects of acid activation in BC properties were evaluated using a range of characterization techniques, including Brunauer–Emmett–Teller (BET) surface area analysis, Fourier transform infrared (FTIR) spectroscopy, scanning electron microscopy (SEM), X-ray diffraction (XRD), Raman spectroscopy, and thermogravimetric analysis (TGA).

Materials and Methods

Materials

Biochar was procured from a biochar plant in John Day, OR, USA, made from wood biomass through the pyrolysis process around 300 °C with a residence time of 25 to 30 minutes. Acid activation of the BC was performed with nitric acid (HNO_3), hydrochloric acid (HCl), phosphoric acid (H_3PO_4), or sulfuric acid (H_2SO_4), all purchased from Thermo Fisher Scientific (Waltham, MA, USA).

Biochar for Acid Activation

Prior to acid activation, the BC from the biochar plant was sieved through a 180 µm mesh to achieve a relatively uniform particle size. To decrease the particle size further, the BC was ball milled in a FlackTek™ speed mixer (Landrum, SC, USA) for 30 minutes at 1000 rpm and labeled as BC_BM. The BC_BM samples were characterized and then treated with acids for acid activation.

Acid Activation of Biochar

In acid activation, biochar was treated with four acids—nitric acid (HNO_3), hydrochloric acid (HCl), phosphoric acid (H_3PO_4), and

sulfuric acid (H_2SO_4)—to compare the effects of different acids. Figure 1 shows the schematic representation of acid-activated biochar (ABC) synthesis. Solutions of 1M (1 mole) from each acid were prepared, and 1.5 g of BC was added to each. The mixtures were magnetically stirred continuously for 2 hours at 60 °C, then left to stand overnight. Afterward, the biochar was thoroughly washed with distilled water, with the pH adjusted to pH 7 during the washing process. The ABC was then dried in an oven at 100 °C for further characterization.

Characterization Techniques

The morphology of the BC before and after the acid activation was imaged using a Phenom XL Desktop scanning electron microscope (SEM; Thermo Fisher Scientific). The imaging was carried out using an accelerating voltage of 5kV in a backscatter electron detector. The effect of acid treatment on functional groups attached to the BC was analyzed using a Nicolet iS50 Fourier transform infrared (FTIR) spectrometer (Thermo Fisher Scientific). The X-ray diffraction (XRD) characterization of the ABC samples was conducted on a benchtop Miniflex 600 diffractometer (Rigaku, Tokyo, Japan). The Brunauer–Emmett–Teller (BET) analysis for surface area of the samples was conducted on an ASAP 2020 physisorption analyzer (Micromeritics Instruments Corp., Norcross, GA, USA) after degassing the samples at 150 °C for 30 minutes. The sample was scanned at a scan rate of 1° per minute from 5° to 60° Bragg angle at 30 kV and 15 mA. A DXR Raman spectrometer (Thermo Fisher Scientific) with an excitation wavelength of 780 nm was used to determine the defect ratio of the ABC samples. The thermal stability of the ABC samples was analyzed using a Discovery TGA 5500 (TA Instruments, New Castle, DE, USA).

Results and Discussion

Characterization of Acid-Activated Biochar

To examine the morphological changes in biochar before and after acid treatment, SEM imaging was performed. Figure 2A shows the SEM image of BC after sieving through a 180 µm mesh, revealing relatively uniform particle sizes. Figure 2B displays the BC after 30 minutes of ball milling, where a significant reduction in particle size can be observed. Figures 2C and 2D present higher magnification images of the BC_BM sample, highlighting the finer structural details.

Biochar samples activated with different acids were characterized to assess the modifications in their surface and bulk properties. Brunauer–Emmett–Teller analysis was conducted on the ABC samples to evaluate the impact of acid activation on the surface area and porosity of the biochar. The BET results for the ABC samples (Table 1) show increases in surface area and micropore volume for biochar treated with HCl, H_3PO_4, and $H2SO_4$ compared to the

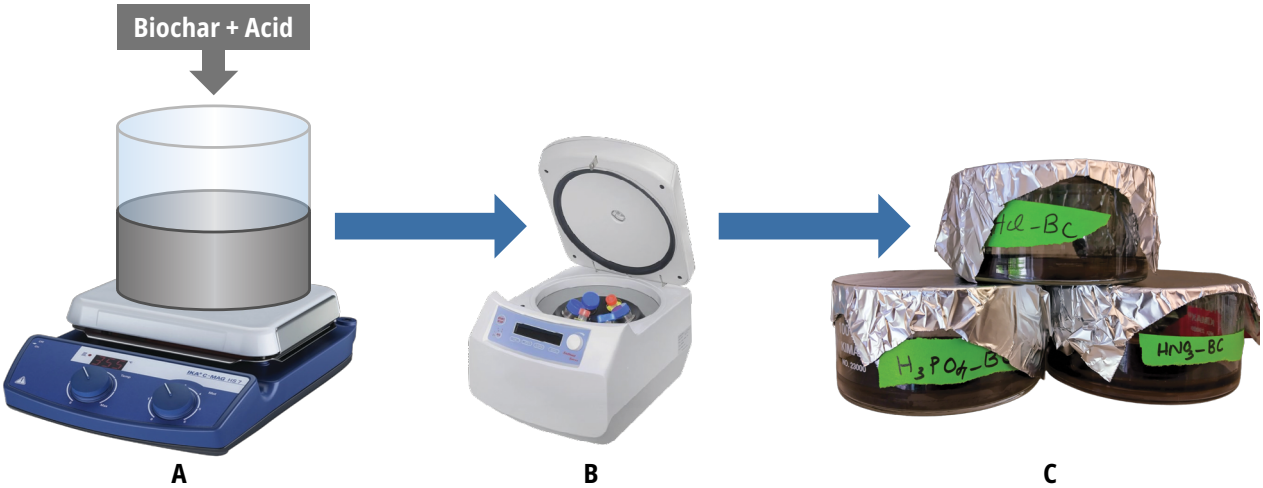

Figure 1.—Schematic showing the preparation of acid-activated biochar using different acids. A: Solutions of 1M (1 mole) of each acid—nitric acid (HNO_3), hydrochloric acid (HCl), phosphoric acid (H_3PO_4), and sulfuric acid (H_2SO_4)—were prepared; 1.5 g of biochar was added to each and magnetically stirred for 2 hours at 60 °C and left to stand for 24 hours. B: Acid-activated biochar was washed several times using a centrifuge to pH 7. C: Biochar was dried in an oven at 100 °C to obtain acid-activated biochar (ABC).

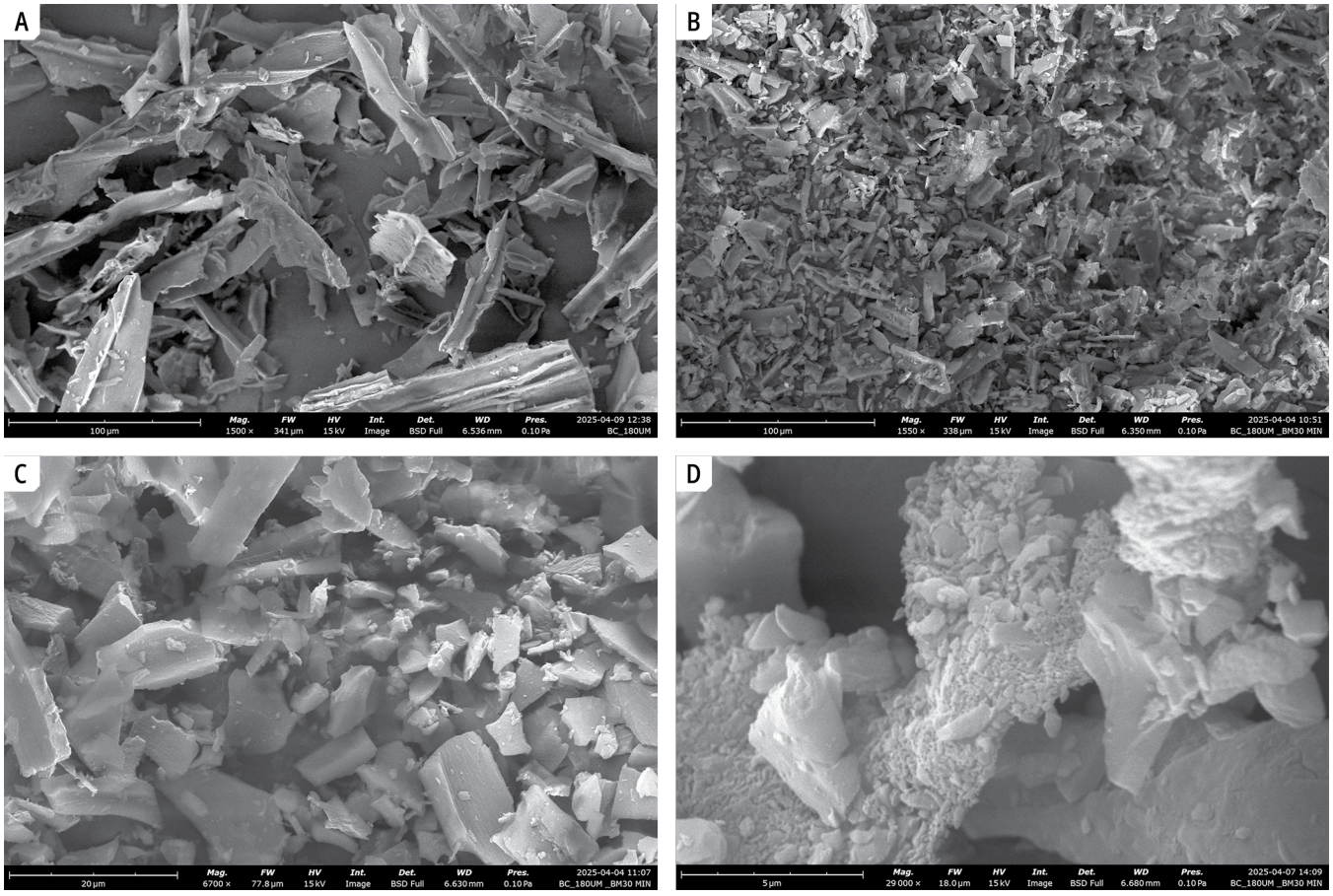

Figure 2.—Scanning electronic microscopy (SEM) images of biochar before acid activation. A: 180 µm mesh-sieved biochar (BC); B, C, D: Ball-milled biochar (BC_BM) for 30 minutes at increasing magnification. Images by Radhika Panickar/Alabama State University.

Table 1.—Summary of Brunauer–Emmett–Teller (BET) analysis of ball-milled biochar (BC_BM) and acid-activated biochar (ABC) samples in 1 mole (1M) solutions

Biochar	Surface area (m^2/g)	Micropore volume (cm^3/g)	Average pore width (nm)	Percent surface area change from BC_BM
BC_BM	5.0810	0.003746	2.63448	
BC_1M_HNO_3	4.6414	0.003115	2.56385	-8
BC_1M_HCl	5.4801	0.005664	0.51862	10
BC_1M_H_3PO_4	6.6586	0.004289	2.53446	34
BC_1M_H_2SO_4	5.3005	0.004054	2.37830	6

BC_BM (neat biochar). Of the four acids, H_3PO_4 treated biochar exhibited the most significant enhancement, with a 34 percent increase in surface area relative to the neat biochar. Chu et al. (2018) reported that pretreating sawdust with H_3PO_4 during biochar synthesis increased the surface area by promoting micropore development, which aligns with the findings of the present study.

The BET analysis shows a negative impact of HNO_3 on the surface area compared to neat BC_BM. It has been reported that BC synthesized at low temperature pyrolysis treated with HNO_3 is more susceptible to collapsing the pore walls

and narrowing the pore volume, which might result in reduced surface area (Nzediegwu et al. 2022). Based on SEM and BET analyses, it can be concluded that other acids in the study were less effective than H_3PO_4 because their harsh oxidative or corrosive effects often damaged the BC porous structure or did not sufficiently promote micropore formation.

The functional groups attached to the biochar before and after acid activation using HNO_3, HCl, H_3PO_4, and H_2SO_4 were analyzed using FTIR spectroscopy. Figure 3 shows the FTIR spectrum of the neat BC_BM compared with ABC. Figure 3A shows the FTIR spectra of BC (180 µm mesh-sieved), BC_BM, and HNO_3-treated BC; the figure inset is a magnified view of the spectral region between 2000 and 600 cm^{-1}. The FTIR spectra of BC and BC_BM were identical, suggesting that ball milling did not affect the surface functional groups of the biochar. The FTIR spectrum of HNO_3-treated BC reveals strong acid functionalization on BC_BM. HNO_3-activated BC_BM exhibited high intensity peaks along with a blue shift, suggesting a strengthening of certain bonds in the ABC. Since the biochar in this study was produced at 300 °C, the organic compounds were not fully decomposed; as a result, after

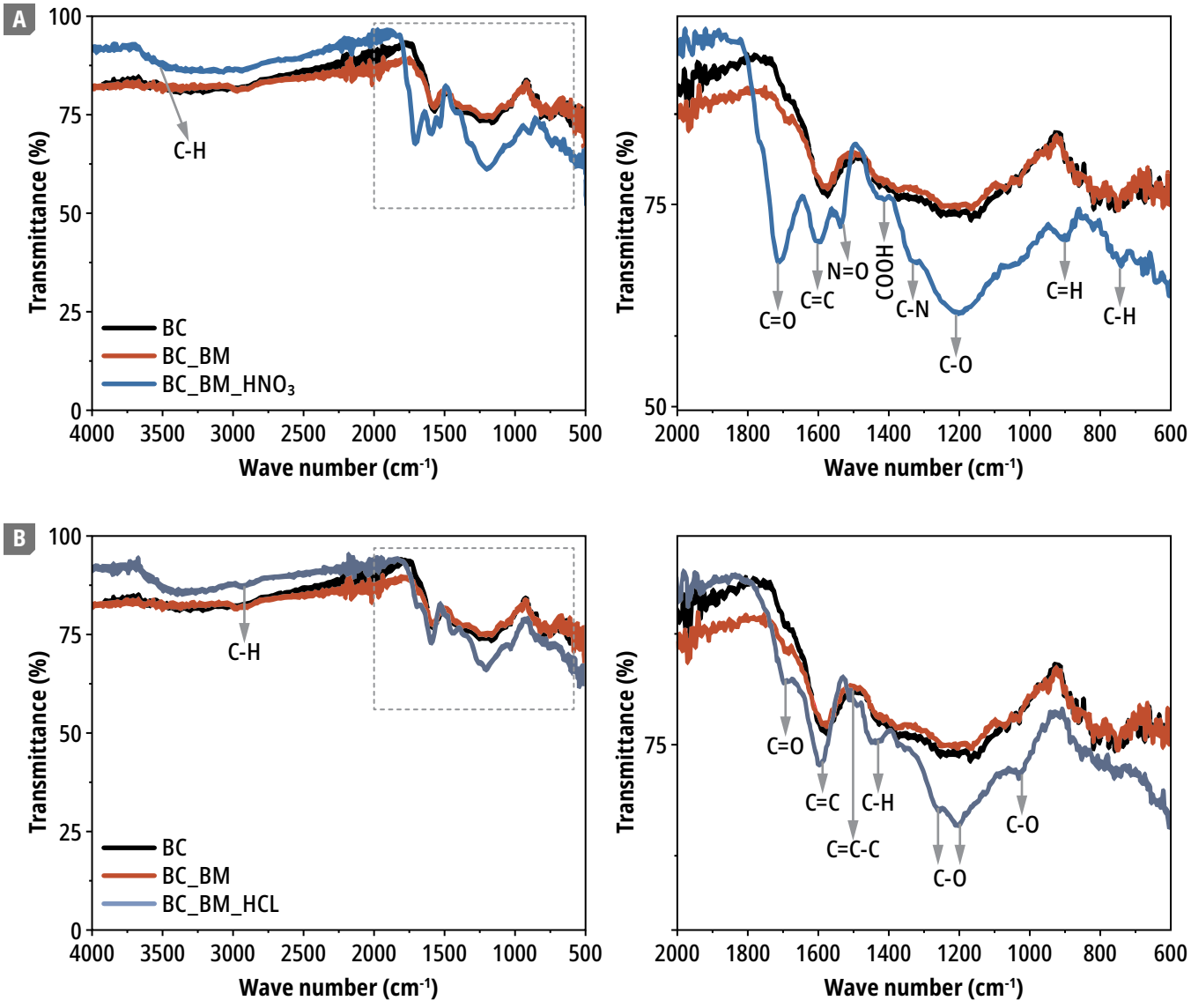

Figures 3A–3B.—Fourier transform infrared (FTIR) spectrum of biochar (BC) compared with ball-milled biochar (BC_BM) and acid-activated biochar. A: HNO_3, B: HCl. Graphs on the right side are magnified views of the spectral regions between 2000 and 600 cm^{-1}. *(continued on next page)*

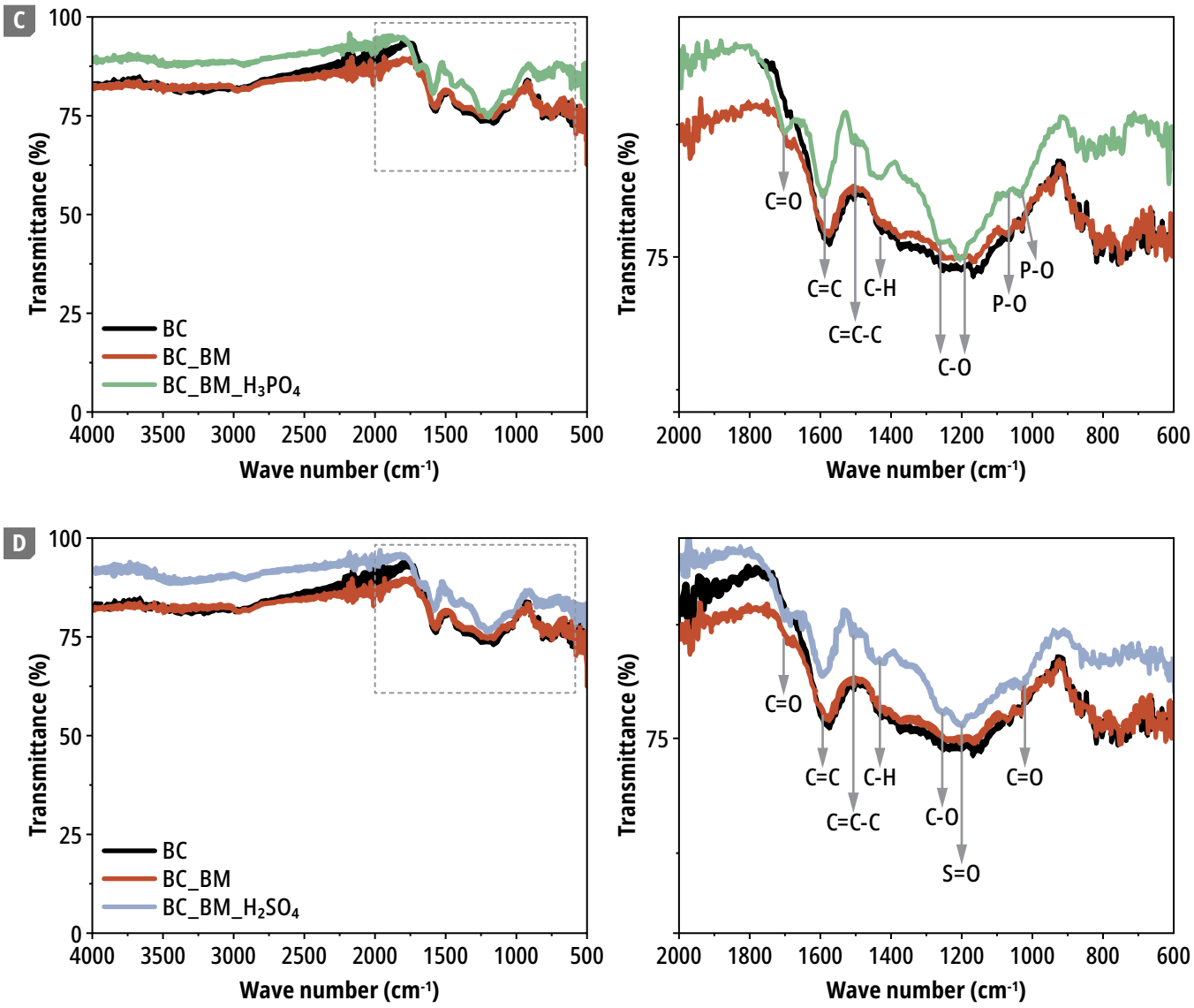

Figures 3C–3D.—Fourier transform infrared (FTIR) spectrum of biochar (BC) compared with ball-milled biochar (BC_BM) and acid-activated biochar. C: H_3PO_4, D: H_2SO_4. Graphs on the right side are magnified views of the spectral regions between 2000 and 600 cm^{-1}.

acid treatment the FTIR spectrum of all ABC showed prominent peaks corresponding to lignin, cellulose, and hemicellulose. Broad peaks around 2933 cm^{-1} were observed corresponding to aliphatic C–H stretching vibrations. Prominent peaks at 1708.6 cm^{-1} and 1602.5 cm^{-1} correspond to the C=O stretching vibration in the carbonyl functional group of cellulose and hemicellulose and C=C stretching vibrations of lignin structure, respectively (Estevez et al. 2013). Nitrogen functional group N=O was observed at 1535.5 cm^{-1} and 1330.6 cm^{-1} in the spectrum, where 1535.5 cm^{-1} indicates the asymmetric stretching vibration and 1330.6 cm^{-1} is most likely the symmetric N=O stretch of nitro groups. A peak at 1505.6 cm^{-1}, attributed to the aromatic ring of guaiacyl-syringyl (GS) lignin, was detected in BC_BM (Sammons et al. 2013); however, this peak disappeared following HNO_3 treatment, likely due to the degradation of lignin's aromatic structures (Armynah et al. 2018).

A peak at 1425.6 cm^{-1} corresponds to the carboxylate groups (COO^- symmetric stretch) or related oxygen-containing functionalities introduced by oxidation. It has been reported that the peak at 1425.6 cm^{-1} also indicates the vibration of the aromatic ring of lignin or C-H

bending in cellulose. The broad peak at 1214 cm^{-1} in biochar indicates the C–O stretching vibrations of oxidized aromatic ethers and phenolic groups, which indicate the presence of lignin-derived structures (Armynah et al. 2018). Peaks at 897.2 cm^{-1} and 744.9 cm^{-1} are assigned to aromatic C–H out-of-plane bending vibrations.

Figure 3B shows BC, BC_BM, and BC treated with HCl FTIR spectra; the figure inset is a magnified view of the spectral region between 2000 and 600 cm^{-1}. BC_BM treated with HCl also exhibited similar FTIR peaks with slight shifts in the values. Apart from the common peaks observed in HCl, activated BC exhibited a right shift in the aromatic lignin peak at 1505.1 cm^{-1} to 1510.6 cm^{-1}, corresponding to a slight rearrangement of lignin's aromatic framework. Broad peaks at 1256.3 cm^{-1} and 1214.4 cm^{-1} were observed, indicating C–O stretching vibrations in aromatic ethers linked to G lignin units and phenolic groups. A C-O stretching vibration peak corresponding to cellulose and hemicellulose was observed at 1028 cm^{-1}.

Figure 3C presents the FTIR spectra of BC, BC_BM, and BC treated with H_3PO_4; the figure inset is a magnified view of the spectral region between 2000 and 600 cm^{-1}. The H_3PO_4-treated biochar displayed similar characteristic peaks with slight shifts. In addition to the common features, new bands appeared at 1076.3 cm^{-1} and 1036.2 cm^{-1}, corresponding to P–O vibrations from phosphate groups. Notably, the aromatic lignin peak shifted from 1505.1 cm^{-1} to 1509.5 cm^{-1}, suggesting a structural rearrangement within the lignin framework (Esteves et al. 2013).

Figure 3D gives the FTIR spectrum of BC, BC_BM, and BC treated with H_2SO_4; the figure inset is a magnified view of the spectral region between 2000 and 600 cm^{-1}. BC_BM treated with H_2SO_4, FTIR spectrum exhibited asymmetric stretching from sulfonic acid groups at 1206.8 cm^{-1} and 1036.6 cm^{-1}. Notably, the aromatic lignin peak shifted from 1505.1 cm^{-1} to 1507.5 cm^{-1}, suggesting a slight structural rearrangement within the lignin framework.

Figure 4 shows spectral overlays of all the ABC samples according to the characterization method. Figure 4A presents the FTIR spectra of all the ABC samples in a single plot for comparison with BC_BM. To evaluate structural changes in biochar following acid activation, XRD analysis was performed. Figure 4B presents the XRD patterns of BC_BM samples treated with the four acids. Broad diffraction peaks observed at 23.44° and 43.08° correspond to the (002) and (100)/(101) planes of graphitic carbon, respectively, indicating the presence of predominantly amorphous carbon. The persistence of these peaks indicates that the amorphous carbon structure remained largely unchanged after acid treatment. Biochar activated with H_3PO_4 and H_2SO_4 exhibited almost similar XRD spectra compared to BC_BM. However, treatment with HCl and HNO_3 led to noticeable reductions in XRD peak intensity. These decreases can be attributed to the higher acidity and stronger demineralizing effect of HCl and HNO_3, which facilitated the removal of crystalline mineral phases and thereby lowered the overall diffraction signal (Wang et al. 2020).

Figure 4C presents the Raman spectra of the ABC samples, analyzed to assess the degree of graphitization following acid treatment. The Raman spectrum exhibited two key peaks: D band at 1363 cm^{-1} and G band at 1584 cm^{-1}. The defect ratio (ID/IG) was calculated from the intensities of the D and G bands. The BC_BM exhibited a high defect ratio of 0.94, whereas acid-treated samples showed lower values. Among them, BC treated with H_3PO_4 displayed the lowest defect ratio, 0.82, indicating the highest degree of graphitization. These results demonstrate that acid treatment removed impurities from the biochar surface, thereby reducing structural defects, enhancing graphitic ordering, and leading to more graphitized carbon in the ABC samples (Pusceddu et al. 2019, Sutar and Jadhav 2024).

The thermal stability of the acid-activated samples was analyzed using thermogravimetric analysis (TGA). Figure 4D shows the TGA thermograms for samples heated in an inert atmosphere up to 900 °C. Table 2 summarizes the TGA analysis of the ABC samples. All ABC samples demonstrated improved thermal stability compared to the BC_BM sample, except for the sample treated with HNO_3. The BC_BM sample exhibited an initial degradation temperature of 345.63 °C, whereas samples treated with HNO_3, HCl, H_3PO_4, and H_2SO_4 showed initial degradation temperatures of 198.14, 358.96, 367.14, and 363.24 °C, respectively. At 900 °C, none of the samples were fully degraded. The recorded weight loss values were 87, 65, 56, 48, and 92 percent for BC_BM and acid-activated BC treated using HNO_3, HCl, H_3PO_4,

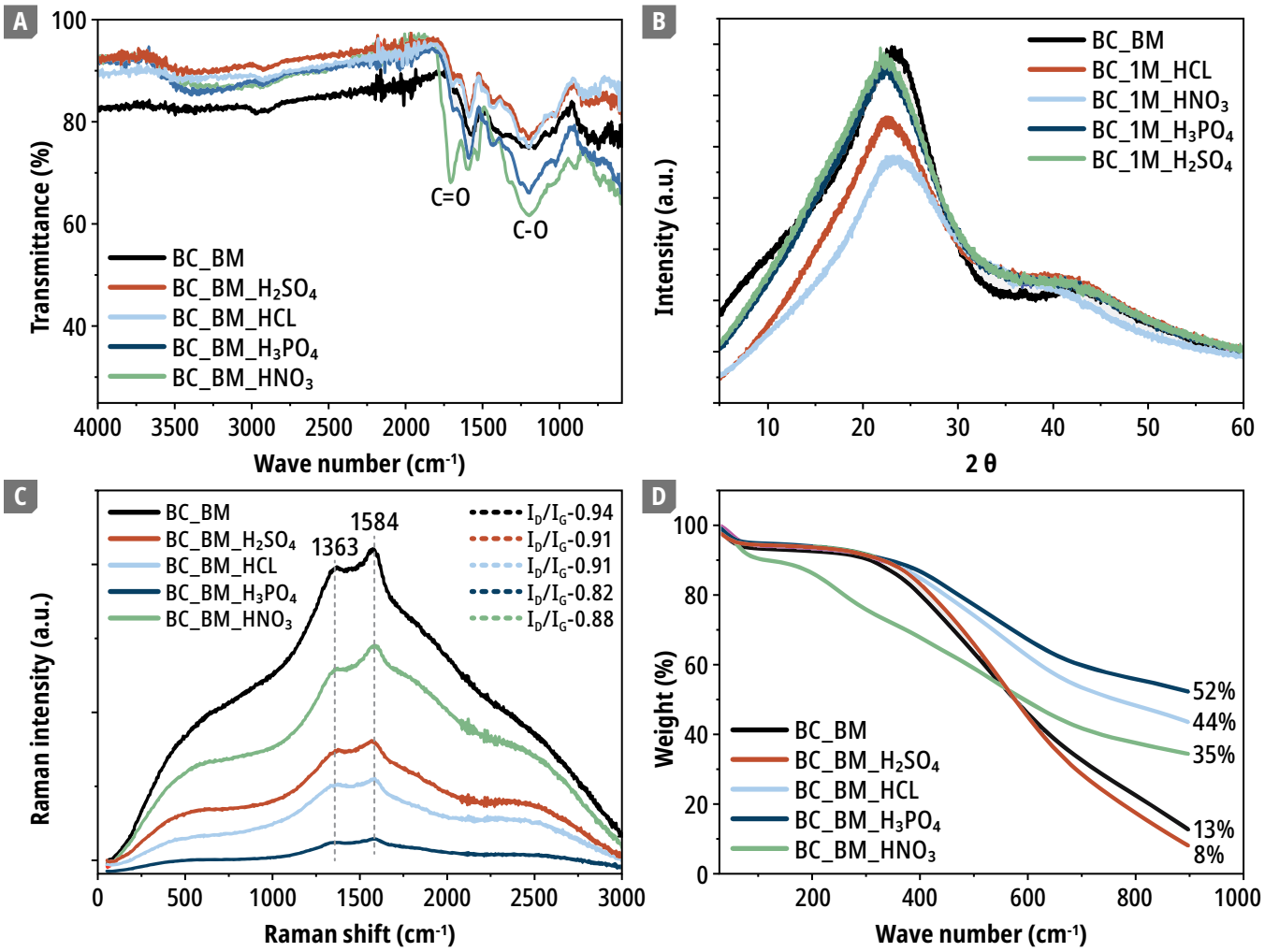

Figure 4.—Characterization of the ball-milled biochar (BC_BM) and acid-activated biochar (ABC) samples. A: Fourier transform infrared spectroscopy (FTIR), B: X-ray diffraction (XRD), C: Raman spectroscopy, and D: thermogravimetric analysis (TGA).

Table 2.—Summary of the thermogravimetric analysis (TGA) of the ball-milled biochar (BC_BM) and acid-activated biochar (ABC) samples

Samples	Initial degradation temperature (°C)	Weight loss (percent)
BC_BM	345.63	87
BC_BM_HNO_3	198.14	65
BC_BM_HCl	358.96	56
BC_BM_H_3PO_4	367.14	48
BC_BM_H_2SO_4	363.24	92

and H_2SO_4, respectively. The results show that, compared to other acid-activated BC samples, the H_3PO_4-treated biochar exhibited a 22 °C increase in initial degradation temperature, corresponding to a 6.23 percent rise and indicating enhanced thermal stability at elevated temperatures. It has been reported that significant oxidation inhibition by phosphorus causes meta phosphate or P-O attached to the carbon, which can improve the oxidation stability of the BC, resulting in improved thermal properties (Zhao et al. 2014).

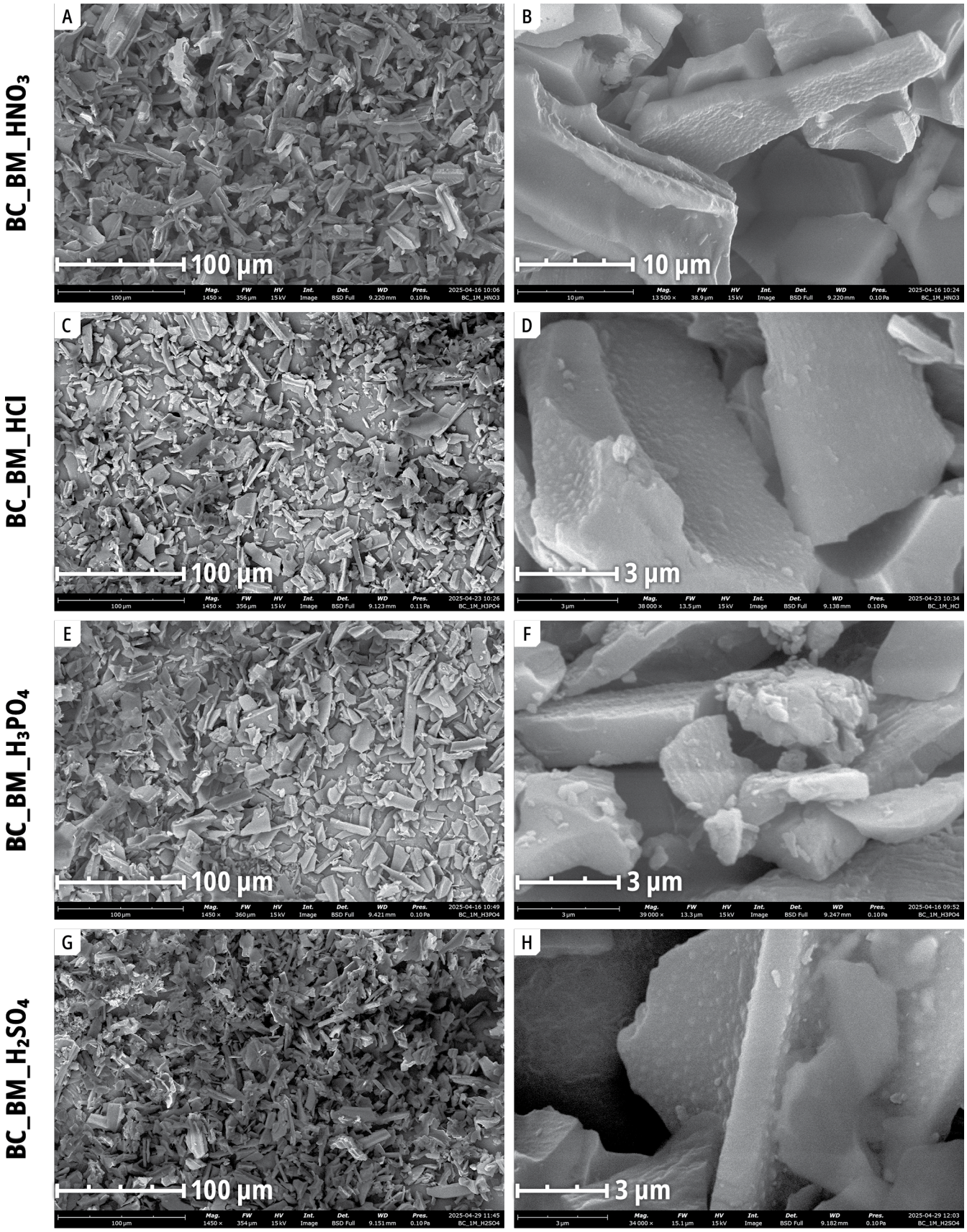

Figure 5.—Scanning electron microscopy (SEM) images of the acid-activated biochar (ABC). A, B: HNO_3; C, D: HCl; E, F: H_3PO_4; and G, H: H_2SO_4. Images by Radhika Panickar/Alabama State University.

The morphology of the BC_BM after acid activation using different acids was imaged using SEM. Figure 5 shows the SEM images obtained for the ABC samples, Figures 5A and 5B show the SEM image of ABC using HNO_3, Figures 5C and 5D show the SEM image of ABC using HCl, Figures 5E and 5F show the SEM image of ABC using H_3PO_4, and Figures 5G and 5H show the SEM image of ABC using H_2SO_4. The SEM images of the ABC samples do not show any significant changes in morphology compared to the original ball-milled BC. Because the BC was synthesized at a very low pyrolysis temperature, the micropores and mesopores were not well formed in the samples (Zhao et al. 2017). However, all the samples exhibited some surface roughness in the higher magnification SEM image after acid activation.

Conclusions and Future Work

Biochar synthesized at a low pyrolysis temperature of 300 °C was subjected to acid activation using nitric acid (HNO_3), hydrochloric acid (HCl), phosphoric acid (H_3PO_4), and sulfuric acid (H_2SO_4). Characterization of the acid-activated biochar demonstrated that acid treatment significantly influences its physical and thermal properties. Fourier transform infrared spectroscopy analysis revealed the emergence of new functional groups and peak shifts, indicating successful chemical modification of the biochar surface. A comparison of the different acids and activation indicated that H_3PO_4 activation resulted in the most notable improvements in the biochar, including enhanced surface area, greater graphitization, and thermal stability.

Future research on acid-activated biochar will focus on developing polymer composites by incorporating ABC as a reinforcing filler in a polymer matrix. Acid-activated biochar at varying weight percentages will be added to polylactic acid (PLA), a biodegradable polymer with promising engineering applications. The PLA/ABC composites will be prepared using dry mixing followed by twin-screw extrusion. The resulting composites will then be investigated for their thermomechanical properties.

Acknowledgments

We thank the Forest Service for funding and providing the biochar for the project and Matt Krumenauer, U.S. Endowment for Forestry and Communities, for providing the biochar and data related to the biochar synthesis.

Literature Cited

Armynah, B.; Atika; Djafar, Z. [et al.]. 2018. Analysis of chemical and physical properties of biochar from rice husk biomass. Journal of Physics: Conference Series. 979(1): 012038. https://doi.org/10.1088/1742-6596/979/1/012038.

Bo, X.; Zhang, Z.; Wang, J. [et al.]. 2023. Benefits and limitations of biochar for climate-smart agriculture: a review and case study from China. Biochar. 5(1): 77. https://doi.org/10.1007/s42773-023-00279-x.

Chu G. ; Zhao J.; Huang Y. [et al.]. 2018. Phosphoric acid pretreatment enhances the specific surface area of biochars by generation of micropores. Environmental Pollution. 240: 1–9. https://doi.org/10.1016/j.envpol.2018.04.003.

da Silva, M.A.; Abdalla Filho, A.L.; Carnier, R. [et al.]. 2025. Low-temperature slow pyrolysis: exploring biomass-specific biochar characteristics and potential for soil applications. Technologies. 13(3): 100. https://doi.org/10.3390/technologies13030100.

Esteves, B. ; Velez Marques, A.; Domingos, I. [et al.]. 2013. Chemical changes of heat-treated pine and eucalypt wood monitored by FTIR. Maderas: Ciencia y Tecnología. 15(2): 245–258. https://doi.org/10.4067/S0718-221X2013005000020.

Gaskin, J.W.; Steiner, C.; Harris, K. [et al.]. 2008. Effect of low-temperature pyrolysis conditions on biochar for agricultural use. Transactions of the ASABE. 51(6): 2061–2069. https://doi.org/10.13031/2013.25409.

Handiso, B.; Pääkkönen, T.; Wilson, B.P. 2024. Effect of pyrolysis temperature on the physical and chemical characteristics of pine wood biochar. Waste Management Bulletin. 2(4): 281–287. https://doi.org/10.1016/j.wmb.2024.11.008.

Leng, L.; Huang, H. 2018. An overview of the effect of pyrolysis process parameters on biochar stability. Bioresource Technology. 270: 627–642. https://doi.org/10.1016/j.biortech.2018.09.030.

Leng, L.; Xiong, Q.; Yang, L. [et al.]. 2021. An overview on engineering the surface area and porosity of biochar. Science of the Total Environment. 763: 144204. https://doi.org/10.1016/j.scitotenv.2020.144204.

Nzediegwu, C.; Naeth, M.A.; Chang, S.X. 2022. Feedstock type drives surface property, demineralization and element leaching of nitric acid-activated biochars more than pyrolysis temperature. Bioresource Technology. 344: 126316. https://doi.org/10.1016/j.biortech.2021.126316.

Pariyar, P.; Kumari, K.; Jain, M.K. [et al.]. 2020. Evaluation of change in biochar properties derived from different feedstock and pyrolysis temperature for environmental and agricultural application. Science of the Total Environment. 713: 136433. https://doi.org/10.1016/j.scitotenv.2019.136433.

Pusceddu, E.; Santilli, S.F.; Fioravanti, G. [et al.]. 2019. Chemical-physical analysis and exfoliation of biochar-carbon matter: from agriculture soil improver to starting material for advanced nanotechnologies. Materials Research Express. 6(11): 115606. https://doi.org/10.1088/2053-1591/ab4ba8.

Roshan, A.; Ghosh, D.; Maiti, S.K. 2023. How temperature affects biochar properties for application in coal mine spoils? A meta-analysis. Carbon Research. 2(1): 1–17. https://doi.org/10.1007/s44246-022-00033-1.

Sammons, R.J.; Harper, D.P.; Labbé, N. [et al.]. 2013. Characterization of organosolv lignins using thermal and FT-IR spectroscopic analysis. BioResources. 8(2): 2752–2767. https://doi.org/10.15376/biores.8.2.2752-2767.

Skic, K.; Adamczuk, A.; Gryta, A. [et al.]. 2024. Surface areas and adsorption energies of biochars estimated from nitrogen and water vapour adsorption isotherms. Scientific Reports. 14: 30362. https://doi.org/10.1038/s41598-024-81030-9.

Sutar, S.; Jadhav, J. 2024. A comparative assessment of the methylene blue dye adsorption capacity of natural biochar versus chemically altered activated carbons. Bioresource Technology Reports. 25: 101726. https://doi.org/10.1016/j.biteb.2023.101726.

Tan, Z.; Yuan, S. 2019. The effect of preparing temperature and atmosphere on biochar's quality for soil improving. Waste and Biomass Valorization. 10(5): 1395–1405. https://doi.org/10.1007/s12649-017-0145-1.

Uroić Štefanko, A.; Leszczynska, D. 2020. Impact of biomass source and pyrolysis parameters on physicochemical properties of biochar manufactured for innovative applications. Frontiers in Energy Research. 8: 138. https://doi.org/10.3389/fenrg.2020.00138.

Wang, Z.; Li, J.; Zhang, G. [et al.]. 2020. Characterization of acid-aged biochar and its ammonium adsorption in an aqueous solution. Materials. 13(10): 2270. https://doi.org/10.3390/ma13102270.

Yaashikaa, P.R.; Senthil Kumar, P.; Varjani, S. [et al.]. 2020. A critical review on the biochar production techniques, characterization, stability and applications for circular bioeconomy. Biotechnology Reports. 28: e00570. https://doi.org/10.1016/j.btre.2020.e00570.

Zhao, L.; Cao, X.; Zheng, W. [et al.]. 2014. Phosphorus-assisted biomass thermal conversion: reducing carbon loss and improving biochar stability. PLoS One. 9(12): e115373. https://doi.org/10.1371/journal.pone.0115373.

Zhao, S.-X.; Ta, N.; Wang, X.-D. 2017. Effect of temperature on the structural and physicochemical properties of biochar with apple tree branches as feedstock material. Energies. 10(9): 1293. https://doi.org/10.3390/en10091293.

FOREST PRODUCTS LABORATORY

https://research.fs.usda.gov/fpl